Proposal for the J-PARC 30-GeV Proton Synchrotron:

Investigating $\bar{d}$+^{12}C nuclear interactions at the J-PARC K1.8 beam line

T. Akaishi[2], C. Curceanu[14], K. Ebata[16], Z. Feng[17], M. Fujita[5], C. Han[7], T. K. Harada[16], T. Hashimoto[1], S. H. Hayakawa[3], Y. Hong[3], Y. Ichikawa[3], T. Isobe[1], K. Itahashi[1], M. Iwasaki[1], S. Kanda[6], R. Kurata[3], D. X. Lin[7], Y. Ma[1], S. Manti[14], R. Murayama[1], M. Niiyama[11], H. Noumi[2], H. Ohnishi[4], S. Okada[13], F. Oura[3], F. Sakuma[1], M. Sasano[1], B. Scavino[9], A. Scordo[14], R. Sekiya[16], C. Seong[3], F. Sgaramella[14], K. Shirotori[2], F. Sirghi[14], D. Suzuki[1], K. Suzuki[2], X. Sun[7], T. Takahashi[6], T. N. Takahashi[2], U. Tamponi[8], M. Tanaka[12], K. Tanida[5], K. Tsukada[15], M. Ukai[6], H. Wang[7], T. Yamaga[6], T. O. Yamamoto[5], Y. Zhang[7], H. Zhang[10]

[1]RIKEN, Wako, 351-0198, Japan
[2]Research Center for Nuclear Physics, Osaka University, Osaka, 560-0043, Japan
[3]Department of Physics, Tohoku University, Miyagi, 980-8578, Japan
[4]Research Center for Accelerator and Radioisotope Science, Tohoku University, Miyagi, 982-0826, Japan
[5]Japan Atomic Energy Agency, Tokai, 319-1195, Japan
[6]KEK, Tsukuba, 305-0801, Japan
[7]Institute of Modern Physics, Chinese Academy of Sciences, Lanzhou, 730000, China
[8]INFN Sezione di Torino, Turin, Italy
[9]Department of Physics and Astronomy, Uppsala University, Sweden
[10]School of Nuclear Science and Technology, Lanzhou University, Lanzhou, 730000, China
[11]Department of Physics, Kyoto Sangyo University, Kyoto, 603-8555, Japan
[12]Faculty of Science and Engineering, Waseda University, Tokyo, 169-8555, Japan
[13]College of Science and Engineering, Chubu University, Kasugai, 487-8501, Japan
[14]Laboratori Nazionali di Frascati dell' INFN, I-00044 Frascati, Italy
[15]Institute for Chemical Research, Kyoto University, Kyoto, 611-0011, Japan
[16]Department of Physics, Kyoto University, Kyoto, 611-0011, Japan
[17]School of Physics and Optoelectronics, South China University of Technology, Guangzhou 510640, China

Executive Summary

As the first step toward understanding antimatter composed of multiple antinucleons, we propose to investigate the antideuteron and its interactions with nucleus using $\bar{d}$ beam at the K1.8 beam line of the J-PARC Hadron Experimental Facility.
The proposed experiment will use the $\bar{d}$+^{12}C reaction to study the multiple $\bar{N}-N$ interactions. There are two main objectives for this experiment: measure the coherent (σ_{CohAnn}) and partial (σ_{ParAnn}) annihilation cross section to derive the optical potential between $\bar{d}$ and ^{12}C nucleus; study multiple $\bar{N}-N$ annihilation mechanism by measuring annihilation phase space via $\pi^{\pm}$ momentum distribution.
In the broader context of the QCD phase diagram, these two observables serve as complementary probes of dense baryonic matter. A strongly attractive $\bar{d}$–nucleus potential would compress the nuclear medium before annihilation, while one-step simultaneous annihilation selectively samples short-range correlated nucleon pairs—both mechanisms pushing the local density toward or beyond $2\rho_0$. Our measurements will thus provide the first direct constraints on QCD matter in the low-temperature, high-density region of the phase diagram—a domain inaccessible to heavy-ion collisions and complementary to neutron-star observations.
The major parameters of this experiment are summarized below:

	Beam line	:	K1.8
Calibration run	Purpose	:	pion multiplicity and momentum calibration for single $\bar{p}-N$ annihilation reaction
	Secondary beam	:	0.9 GeV/c $\bar{p}$
	Reaction	:	$\bar{p}$+^{12}C
	Main apparatus	:	K1.8 beam line
	Beam time	:	92 kW $\times$ 2 days
Physics run	Purpose	:	Derive $\bar{d}$–^{12}C optical potential and study multiple $\bar{N}-N$ annihilation mechanism
	Secondary beam	:	1.8 GeV/c $\bar{d}$
	Reaction	:	$\bar{d}$+^{12}C
	Main apparatus	:	KURAMA dipole spectrometer
	Beam time	:	92 kW $\times$ 40 days (Proposed statistics: 1×10^6 $\bar{d}$ beam particles)

Contents

1 Introduction

Antimatter has held a significant position within both the scientific community and popular culture for many years. It has captured attention ranging from testing CPT violation [1, 2] to its portrayal in Hollywood movies [3], symbolizing humanity's unrelenting pursuit of the unknown. The investigation into antimatter and its dynamic interplay with matter remains intricately intertwined with one of contemporary physics' most profound enigmas: the antimatter-matter imbalance. Numerous investigations into antiprotons ($\bar{p}$) and their interaction with matter have been undertaken to address this puzzle [4].

However, the exploration of antinuclei composed of multiple antinucleons, such as the antideuteron ($\bar{d}$), remains relatively unexplored territory. For instance, only absorption cross sections on heavy targets are reported at 13.3 GeV/c and 25 GeV/c without information about their reaction products as shown in Fig. 1 [5, 6]. A recent study by the ALICE collaboration shown in Fig. 2 provides the total inelastic cross section between $\bar{d}$ and the averaged detector materials ($< A >= 17.4$ and $< A >= 31.8$) as effective targets, without details about the reactions [7].

As a foundational step toward understanding antimatter composed of multiple antinucleons, we propose to investigate the antideuteron using a $\bar{d}$ beam at the K1.8 beam line of the J-PARC Hadron Experimental Facility. In this proposal, we aim to address the following topics:

1. How does $\bar{d}$ interact with nucleus? By adding one more antinucleon, how will the $\bar{d}-$nucleus potential differ from $\bar{p}-$nucleus?

2. How will the antinucleus annihilate with nucleus? Will the two antinucleons inside $\bar{d}$ annihilate with nucleons from nucleus independently or simultaneously?

The proposed experiment will be conducted at the K1.8 beam line of the J-PARC Hadron Experimental Facility. The $\bar{d}$ beam momentum is set to 1.8 GeV/c in order to maximize the sensitivity of the $\bar{d}-$nucleus optical potential [9]. A 10 cm thick ^{12}C graphite target will be used to enhance luminosity. A dipole magnet spectrometer, KURAMA, will detect the reaction products. The detailed experimental setup and the physics motivation are described in the following sections.

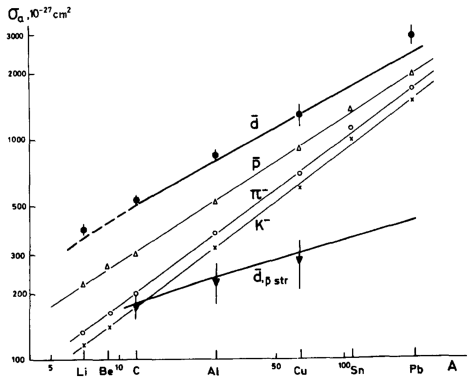

(a) $\bar{d}$ absorption cross section with various targets at 13.3 GeV/c [5].

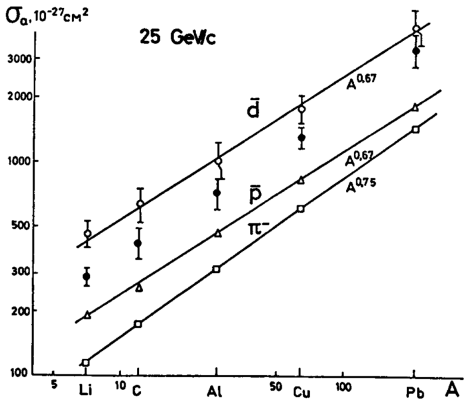

(b) $\bar{d}$ absorption cross section with various targets at 25 GeV/c [6].

Figure 1: $\bar{d}$ absorption cross section measured in 1970s at JINR.

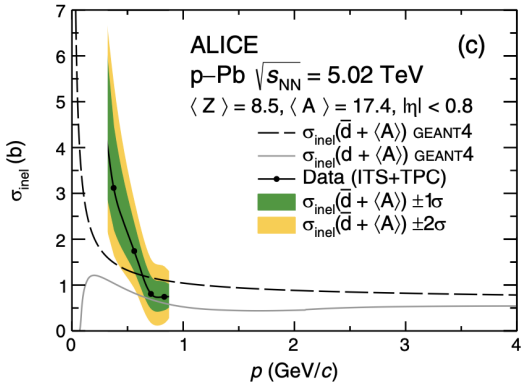

(a) $\bar{d}$ inelastic cross section with P $<$ 1.0 GeV/c.

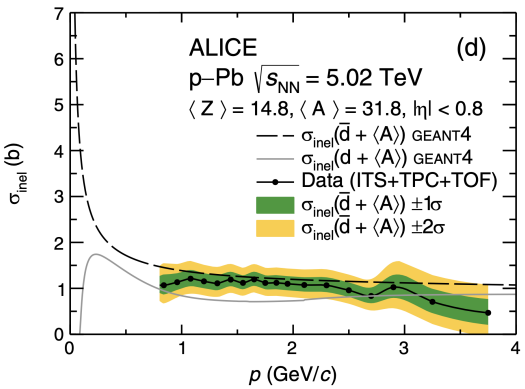

(b) $\bar{d}$ inelastic cross section with P $>$ 1.0 GeV/c.

Figure 2: Inelastic cross section of $\bar{d}$ on ALICE detector as effective target [7].

2 Physics Motivation

In this section, we will discuss the physics motivation behind the proposed experiment. The main topics to be addressed are the $\bar{d}-$nucleus optical potential and the multiple $\bar{N} - N$ annihilation mechanism. The effectiveness of the proposed method will be demonstrated through calculations using the GiBUU package [23].

2.1 Study $\bar{d}-$nucleus Optical Potential

The interaction between antimatter and matter has been a topic of fundamental importance since the discovery of the antiproton in 1955 [8]. Within the framework of Relativistic Mean Field Theory (RMF), the $\bar{p}-$nucleus interaction is expected to be extraordinarily strong due to the flip of G-parity. This flip results in both the scalar and vector potentials becoming attractive, a situation that is usually canceled out in the case of nucleons. A calculation performed exploiting the G-parity flipping returns a potential of of $V \sim -600$ MeV [9].

However, experimental results from both $\bar{p}$-atomic X-ray measurements [10, 11] and $\bar{p}-$nucleus elastic scattering experiments [12] suggest a much weaker interaction, with $V \sim -100$ MeV. One possible explanation for this discrepancy is the large probe distance in both approaches, which makes them sensitive only to the long-range part of the potential. In contrast, the $\bar{p}$ absorption cross section is expected to be more sensitive to the short-range part by penetrating into the nuclear medium and causing absorption. For instance, $\bar{p}$ at 0.6 GeV/c can reach an average of 50% nuclear density before absorption occurs. In this case, the potential is derived as $V \sim -150$ MeV [9].

Another important factor contributing to the deviation from the RMF prediction is the short lifetime of the $\bar{p}-$nucleus system. Regardless of the experimental approach mentioned above, the virtual potential obtained so far consistently shows $W \geq 100$ MeV. Such a strong virtual potential (i.e. the short lifetime) makes it difficult for the $\bar{p}$ nucleus state to reach an equilibrium state before annihilation, which is required by the RMF prediction.

While we have some understanding of the $\bar{p}-$nucleus interaction, the $\bar{d}-$nucleus interaction remains an open question. The $\bar{d}$ nucleus is composed of two antinucleons, making it a unique system for studying multiple $\bar{N} - N$ interactions. If we assume the $\bar{d}-$nucleus system has a similar lifetime to that of the $\bar{p}-$nucleus system, a linear extrapolation from the $\bar{p}-$nucleus potential gives $V - 200 \sim -300$ MeV due to the presence of two attractive centers. This raises the question: Will such a strong attractive potential modify the nucleus structure and the lifetime of the $\bar{d}-$nucleus system? This is one of the key questions we aim to address in this proposal.

In order to investigate quantitatively the $\bar{d}-$nucleus interaction, we will utilize GiBUU, a transport model-based calculation package developed by Giessen University, Germany [23]. GiBUU has been widely used to study $\bar{p}-$nucleus interactions, showing impressive agreement with experimental data [9]. Thanks to the kind support of Dr. K. Gallmeister of the GiBUU group, a $\bar{d}$ beam is now available in the GiBUU package.

To motivate and support our proposal, we performed calculations for the $\bar{d}$+^{12}C reaction with different strengths for the real part of the optical potential. We found that the ratio between partial (σ_{ParAnn}) and coherent (σ_{CohAnn}) annihilation cross sections is very sensitive to the strength of the optical potential. Here, partial annihilation refers to the reaction where only one antinucleon from $\bar{d}$ annihilates with a target nucleon, while coherent annihilation refers to the reaction where both antinucleons from $\bar{d}$ annihilate with target nucleons.

More specifically, for a $\bar{d}$ beam at 1.8 GeV/c, if we assume $V = -150$ MeV between $\bar{N}-$nucleus as derived from $\bar{p}-$nucleus absorption experiment data, the ratio $\sigma_{ParAnn}/\sigma_{CohAnn}$ is approximately 2.8. If we set $V = -300$ MeV between $\bar{N}-$nucleus, the ratio $\sigma_{ParAnn}/\sigma_{CohAnn}$ becomes 1.6, indicating a sensitive dependence. This observation suggests that the ratio between these two cross sections can be used to derive the strength the $\bar{d}-$nucleus optical potential.

From an intuitive perspective, the sensitivity of the ratio $\sigma_{ParAnn}/\sigma_{CohAnn}$ regarding the $\bar{d}-$nucleus optical potential becomes apparent when considering the attractive force between the $\bar{d}$ and the nucleus. A stronger force draws the antinucleons nearer to the nucleus, consequently increasing the likelihood of coherent annihilation. [1] A strongly attractive $\bar{d}$–nucleus potential would compress the nuclear medium before annihilation, probing the local density toward or beyond $2\rho_0$.

2.2 Investigate Multiple $\bar{N} - N$ Annihilation Mechanism

Another interesting topic to be addressed in this experiment is the multiple $\bar{N} - N$ annihilation mechanism. The $\bar{d}$+^{12}C reaction provides a unique opportunity to study how two antinucleons annihilate with nucleons. Understanding this process is crucial for revealing the dynamics of antimatter composed of multiple antinucleons.

To facilitate the discussion, we first categorize the $\bar{d}$+^{12}C annihilation into two main types based on the number of participating antinucleons: partial annihilation, where only one antinucleon from the $\bar{d}$ annihilates with a target nucleon; and coherent annihilation, where both antinucleons from the $\bar{d}$ annihilate with target nucleons.

For coherent annihilation, the mechanism by which both antinucleons annihilate can follow three distinct scenarios, each characterized by different dynamics and phase space:

1. **Two-Step Independent Annihilation**: This involves two independent $\bar{N} - N$ pairs, each annihilating without affecting the other, akin to having two separate $\bar{p} - p$ annihilations. The total phase space is approximately the sum of two individual $\bar{N} - N$ annihilation phase spaces.

2. **Correlated Cascade Annihilation**: In this scenario, one of the mesons produced from the first $\bar{N} - N$ annihilation is absorbed by the second pair before their reaction. The sequence of reactions is: $\bar{N} + N \to (n-1)\pi$, $\pi + \bar{N} \to \bar{\Delta}$ (or $\pi + N \to \Delta$), and $\bar{\Delta} + N \to n\pi$ (or $\Delta + \bar{N} \to n\pi$). Consequently, the second annihilating pair will have a larger phase space available for annihilation reaction due to the increase in total energy from the absorbed meson.

3. **One-Step Simultaneous Annihilation**: If both $\bar{d}$ and ^{12}C are in a short-range correlated (SRC) state during $\bar{d} - 2N$ annihilation, all six $\bar{q} - q$ valence quark pairs can participate simultaneously,

[1] One should note that if the so obtained potential between $\bar{d}$ and nucleus is not so extraordinarily strong that the distortion for the $\bar{d}$ and nucleus wave function are negligible, the $\bar{d}$+^{12}C coherent annihilation cross section can be used to derive the $\bar{d}$ radius for the first time, which is a key to allow us to test the nuclear force universality.

and the annihilation phase space can expand up to ∼4.5 GeV. This extreme case will produce pions with high momentum beyond the kinematic limits of the other two scenarios.

Fig. 3 summarizes these key annihilation modes and their characteristics in the $\bar{d}$+^{12}C reaction. These different mechanisms lead to distinct experimental signatures, particularly in the momentum distributions of the produced pions. The kinematic constraints governing the π momentum distribution are directly linked to the annihilation phase space, which scales with the total energy available. Therefore, by measuring the π momentum distribution, especially in the high-momentum tail region, we can disentangle their relative contributions and identify which annihilation mechanism dominates as explained below.

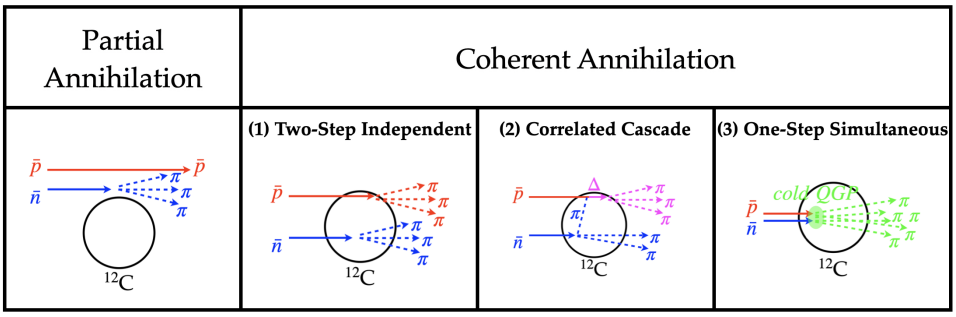

Figure 3: Summary of the different annihilation scenarios and their expected characteristics.

At first glance, all three scenarios produce high-multiplicity final states, making them hard to separate. However, well-studied $\bar{p}-p$ annihilation provides guidance. As shown in Figs. 4 and 5, multiple $\pi^{\pm,0}$ final states dominate $\bar{p}-p$ annihilation at rest [22]. A Gaussian fit to Fig. 4 yields a mean π multiplicity of 5.01 and $\sigma = 1.04$. The $\pi^{\pm,0}$ momentum distribution in Fig. 5 resembles a phase-space distribution, suggesting $\bar{p}-p$ annihilation is a reconfiguration of $\bar{q}-q$ pairs with approximately equal probability.

This motivates using the π momentum spectrum to distinguish the three $\bar{d}$+^{12}C coherent-annihilation scenarios. The total phase space is set by the initial total energy, and the π multiplicity scales with the energy available to the annihilation partners. By analogy with $\bar{p}-p$ at rest, we model the one-step simultaneous case with

$$\begin{aligned} \text{multiplicity} &= \frac{E_{\text{tot}}(\bar{d}+2N)}{m(\bar{p}+p)} \times 5.01, \\ \sigma &= \frac{E_{\text{tot}}(\bar{d}+2N)}{m(\bar{p}+p)} \times 1.04, \end{aligned} \tag{1}$$

where 5.01 and 1.04 are the mean and standard deviation of the π multiplicity in $\bar{p}-p$ annihilation at rest. For correlated cascade annihilation, the total energy of the second pair is increased by absorption of a pion from the first annihilation, modeled by forming a $\bar{\Delta}+N$ (or $\Delta+\bar{N}$) system with a random first-step pion.

The expected $\pi^{\pm}$ momentum spectra for the three scenarios are shown in Figs. 6–8. Two-step independent annihilation, with phase space of order 2.24 GeV (for $\bar{p}$ at 0.9 GeV/c), extends up to ∼1.6 GeV/c. One-step simultaneous annihilation roughly doubles the phase space (∼4.5 GeV), producing a broader spectrum beyond the $\bar{p}-p$ kinematic limit. Correlated cascade lies in between.

We further validate the method using GiBUU with default parameters tuned to $\bar{p}$ data. The primary (generator-level) π momentum distributions for partial and coherent annihilation in $\bar{d}$+^{12}C are shown in Figs. 9 and 10. The small excess above 1.6 GeV/c in partial annihilation (Fig. 9) is due to Fermi motion and is at the ∼10% level compared to the coherent yield beyond that threshold (Fig. 10). The

high-momentum tail in the coherent sample arises from correlated cascade in GiBUU because GiBUU does not currently include the one-step simultaneous mechanism.

Finally, observing the one-step simultaneous component would provide a unique probe of SRC in spatial distributions for both $\bar{d}$ and ^{12}C. SRC has primarily been studied in momentum space via back-to-back high-momentum nucleons in electron scattering [13]. In our case, one-step simultaneous annihilation requires very tight spatial overlap of the $\bar{d}$+^{12}C wave functions, offering direct sensitivity to SRC in coordinate space. One-step simultaneous annihilation selectively samples short-range correlated nucleon pairs, providing complementary constraints on QCD matter in the low-temperature, high-density region—a domain inaccessible to heavy-ion collisions.

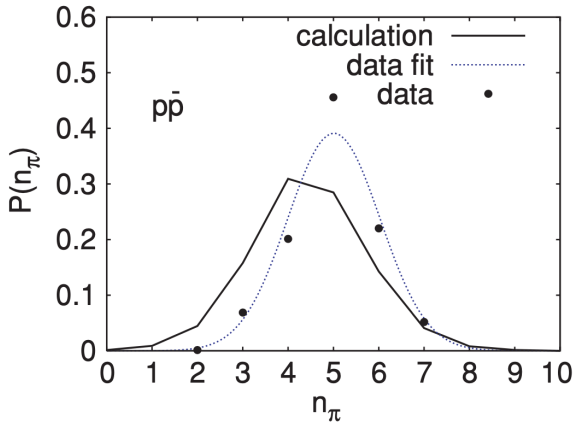

Figure 4: π multiplicity from $\bar{p}-p$ annihilation at rest.

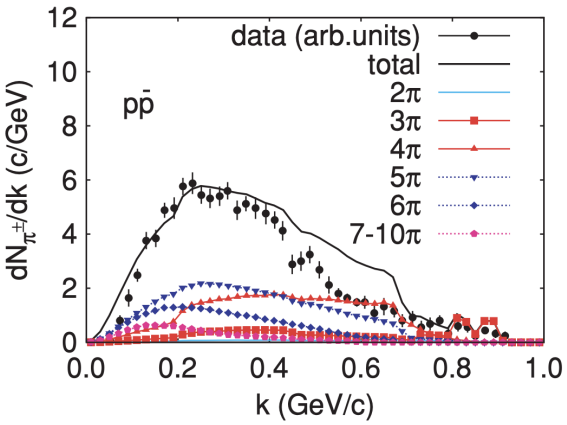

Figure 5: π momentum distribution from $\bar{p}-p$ annihilation at rest.

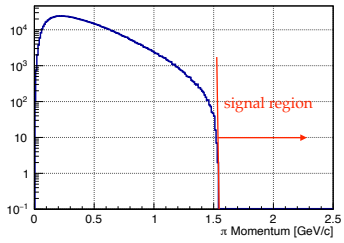

Figure 6: $\pi^{\pm}$ momentum from Two-Step Independent Annihilation with 10^6 $\bar{d}$ on ^{12}C.

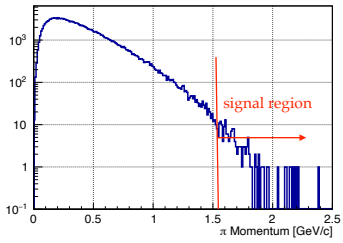

Figure 7: $\pi^{\pm}$ momentum from Correlated Cascade Annihilation with 10^6 $\bar{d}$ on ^{12}C.

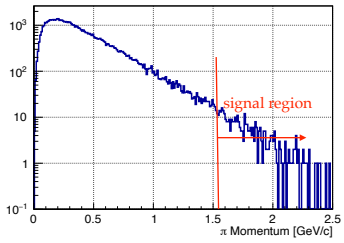

Figure 8: $\pi^{\pm}$ momentum from One-Step Simultaneous Annihilation with 10^6 $\bar{d}$ on ^{12}C.

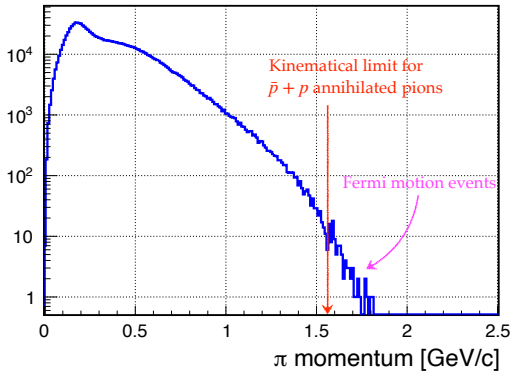

Figure 9: π momentum from $\bar{d}$+^{12}C partial annihilation (primary).

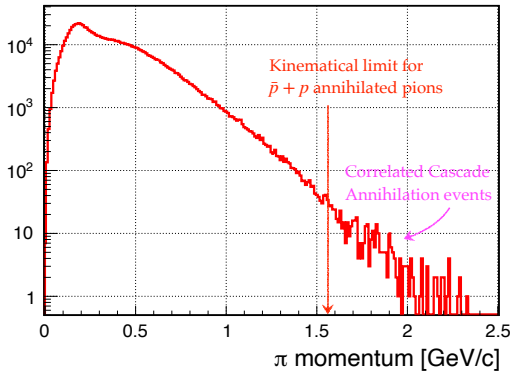

Figure 10: π momentum from $\bar{d}$+^{12}C coherent annihilation (primary).

3 Experimental Setup

This section describes the experimental setup for the proposed $\bar{d}$+^{12}C reaction experiment. The setup consists of a dipole type spectrometer with KURAMA magnet, a graphite target and tracking detectors. The total thickness of the graphite target is determined by GiBUU to be 10 cm, in order to fully react with the $\bar{d}$ beam particles. To minimize the the probability of successive partial annihilation, which can fake a coherent annihilation and contributes as systematic uncertainty in the derivation of the σ_{ParAnn} and σ_{CohAnn}, the target will be sliced into 10 thin plates with 1 cm thickness with 1 cm spacing between them. [2] According to GiBUU, with the proposed 1×10^6 $\bar{d}$ beam particles on the graphite target, we can expect 1.3×10^5 coherent annihilation and 4.0×10^5 partial annihilation reaction events, respectively.

3.1 $\bar{d}$ Beam at K1.8 Beam Line

In a pre-study (J-PARC T108) conducted by one of the authors, M. Ukai, the existence of antideuteron beam has been confirmed and optimized. As shown in Fig. 11a, the antideuteron can be identified by its online Time-of-Flight (TOF) using a small IFV setting (2.2 mm). Further $\bar{d}$ yield optimization by scanning IFV and beam momentum is listed in Fig. 11b. We can see that by choosing the optimal beam momentum of 1.8 GeV/c and IFV of 7.0 mm, a $\bar{d}$ yield of $\sim$ 1.31 $\bar{d}$/spill ($\sim$ 4.24 seconds) can be obtained at 92 kW beam power. To accumulate proposed 10^6 $\bar{d}$ beam particles, a total of 40 days of beam time (92 kW) is required.

We would also like to point out that the production mechanism of $\bar{d}$ at energies below 2.0 GeV/c using high energy protons is still largely unknown [15]. A detailed scan of the $\bar{d}$ yield, along with beam transportation calculations for the K1.8 beam line, could provide some insight into this topic and help us to test the coalescence model.

Another interesting direction waiting to be explored is that according to Ref. [16], the antideuteron yield will be approximately an order of magnitude higher at 6.0 GeV/c. However, as the first experiment to investigate antimatter-matter interactions, we will focus on the $\bar{d}$ physics with relatively low momentum and leave it for future exploration.

[2] This configuration enables us to identify the annihilation vertex for each target plate and effectively reject successive partial annihilation events occurring across multiple plates. The background contribution from successive partial annihilation on the same target plate, which cannot be experimentally distinguished, is estimated to be less than 5% of the final results.

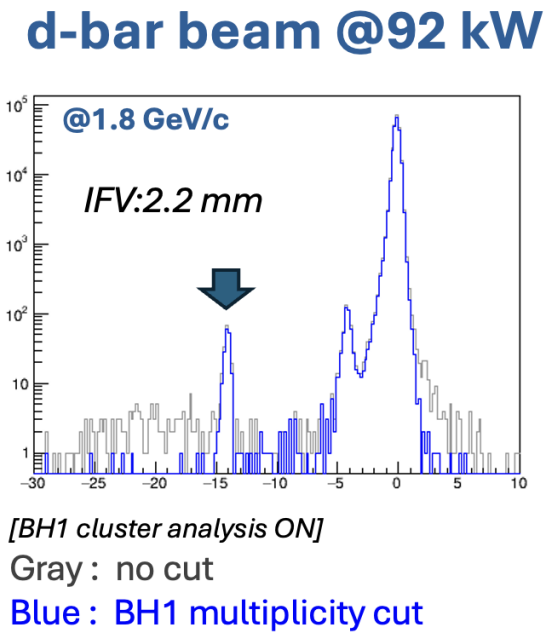

(a) K1.8 beam line TOF, from which the $\bar{d}$ particles are clearly identified.

Summary table of d-bar beam yield

primary proton energy: 30 GeV
primary proton intensity: 81 $\times 10^{12}$ /spill (92 kW)
Primary target : Au 66 mm thickness (50% loss)
Repetition :4.24 s

time	IFV opening [mm]	d-bar rate counts/spill	Total beam rate counts/spill	Corresponding p-bar rate Counts/spill
1.8 GeV/c	2.2	0.56 ± 0.05	0.8k	2.06M
	5.0	0.92 ± 0.07	5.8k	
	7.0	1.31 ± 0.17	38k	
	9.0	1.35 ± 0.16	108k	
1.5 GeV/c	2.2	0.15 ± 0.02	1.5k	1.16M
	5.0	0.21 ± 0.02	18k	
1.3 GeV/c	2.2	0.033 ± 0.005	1.8k	0.60M

Total beam rate => singles rate of timing counter at experimental target area

(b) Summary table of the $\bar{d}$ yield and other relevant parameters. We propose to use the setting with beam momentum of 1.8 GeV/c and IFV of 7.0 mm to optimize the $\bar{d}$ yield and signal to noise ratio.

Figure 11: (a) TOF identification and (b) yield/summary table.

3.2 KURAMA Dipole Spectrometer

To fully utilize the antideuteron beam with very low intensity as described in Section 3.1, we propose an experimental setup as shown in Fig. 12. The central component of the dipole spectrometer is the KURAMA magnet, which is characterized by a large acceptance and a high magnetic field of 0.78 T. The KURAMA magnet has a gap of 80 cm in height, 100 cm in width and 80 cm in length. The momentum resolution of the KURAMA magnet has been demonstrated as $\sim 3\%$ (FWHM) in a previous experiment at J-PARC [24]. For the detailed design of each detector, please refer to the following subsections.

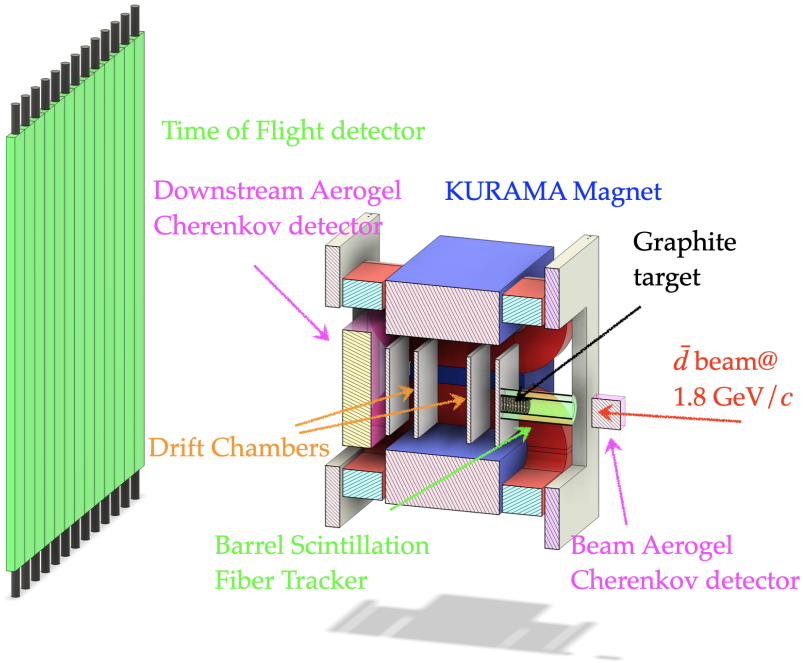

Figure 12: Cross sectional view of the experimental setup. A 10-cm sliced graphite target fully absorbs the $\bar{d}$ beam. Drift chambers track charged particles upstream and downstream. A Barrel Scintillation Fiber Tracker covers the central region, while a forward TOF wall detects forward particles. Beam Aerogel Cherenkov detector suppresses beam background and downstream Aerogel Cherenkov detector rejects false high-momentum $\pi^{\pm}$ events from combinatorial and $\bar{p}$, $\bar{d}$ backgrounds.

3.2.1 Drift Chambers

Four sets of plane type drift chambers will be installed within the KURAMA magnet to track downstream charged particles from the annihilation reaction, with two additional sets of drift chambers placed upstream of the target to cover the backward region. Each set of drift chambers will consist of X-X', U-U', and V-V' layers. This configuration is designed to maximize acceptance of the annihilation products while providing precise momentum measurements for charged particles. The drift chambers will achieve a spatial resolution of 100 μm, enabling a momentum resolution of $\sim 3\%$ (FWHM) for particles with momentum up to 1.8 GeV/c.

3.2.2 Barrel Scintillation Fiber Tracker

The Barrel Scintillation Fiber Tracker will surround the sliced graphite target to capture $\bar{d}$+^{12}C reaction products in the central angular region. This system plays a critical role in precisely measuring the $\sigma_{ParAnn}/\sigma_{CohAnn}$ ratio, which is essential for deriving the $\bar{d}$–^{12}C optical potential and understanding multiple $\bar{N}-N$ annihilation mechanisms.

The tracker consists of two components: an inner tracker with a diameter of 10 cm and an outer tracker with a diameter of 20 cm. Each tracker is constructed using 1 mm diameter scintillation fibers (Kuraray SCSF-78M), which are connected to 8×8 array-type Multi-Pixel Photon Counters (MPPCs) (Hamamatsu S13361) as photon sensors. Both the inner and outer trackers feature four layers of fibers, oriented in $\pm 45^\circ$ configurations, to provide comprehensive 3D tracking information. This design ensures a position resolution of approximately 100 μm, sufficient for handling high-multiplicity events and achieving $\leq 20\%$ uncertainty in the optical potential measurement.

The Barrel Scintillation Fiber Tracker's large acceptance, covering nearly 4π solid angle, enables precise tracking of multiple charged particles from annihilation events. This capability is crucial for quantifying charged particle multiplicities per event, distinguishing between partial and coherent annihilation processes, and disentangling annihilation mechanisms such as Two-Step Independent, Correlated Cascade, and One-Step Simultaneous Annihilation. The tracker will provide the necessary precision to constrain the $\bar{d}$–^{12}C optical potential and explore the dynamics of multiple $\bar{N} - N$ interactions.

3.2.3 Downstream Aerogel Cherenkov Detector

To suppress false high-momentum $\pi^{\pm}$ events caused by combinatorial background and to provide robust suppression of $\bar{p}$ and $\bar{d}$ background, a downstream aerogel Cherenkov detector will be positioned at the exit of the KURAMA magnet. This detector will actively identify outgoing charged pions with momentum $P_\pi \geq 0.5$ GeV/c using an aerogel radiator with a refractive index of $n = 1.04$.

The detector will adopt a modular design, consisting of 100 modules. Each module contains a 10 cm $\times$ 10 cm $\times$ 2 cm aerogel radiator and four Multi-Pixel Photon Counters (MPPCs) on each side. This design ensures a pion detection efficiency of $\geq 95\%$ and a background suppression efficiency of $\geq 99\%$ for $\bar{p}$ and $\bar{d}$ particles. The contamination from background events is expected to be reduced to less than 5% of the signal yield, enabling clean identification of annihilation products, particularly pions from independent or simultaneous antinucleon annihilation.

The downstream aerogel Cherenkov detector is an essential component for ensuring clean momentum measurements and supporting the identification of annihilation products, especially in the high-momentum region. This detector will play a critical role in achieving the physics goals of the experiment, including the study of multiple $\bar{N} - N$ annihilation mechanisms and the search for potential cold quark-gluon plasma signatures.

3.2.4 Forward TOF Wall

A forward scintillation counter wall (FwdTOF) with 500 cm width and 300 cm height is placed at 300 cm of the downstream from the KURAMA magnet center to measure the charged particles in the forward direction. The acceptance and PID capability of the FwdTOF wall will be given in the Section 4.

3.3 Experimental Trigger

Due to the low intensity of the $\bar{d}$ beam ($0.1 \sim 1$ Hz, to be optimized), we will use $beam \otimes \overline{Aerogel}$ as experimental trigger to record all $\bar{d}$ events unbiasedly. The *beam* trigger will be generated by the beam line counter installed in K1.8 beam line, while the $\overline{Aerogel}$ stands for anti-coincidence for the Aerogel counter installed in the upstream of the graphite target to suppress the background beam particles such as $\pi^-/K^-/\bar{p}$.

4 Results and Discussion

To estimate the acceptance and resolution of the experimental setup, we implemented the complete configuration in the GEANT4 simulation package and performed realistic event reconstructions using the simulated detector signals. To gain further insights into the real experimental challenges, we employed the GiBUU calculation as our event generator. This provides us with an understanding of the effects of high multiplicity and neutral particles, such as π^0.

Particle identification (PID) with our proposed setup is illustrated in Fig. 13 including detector resolution and acceptance. PID relies on the momentum and $1/\beta$ of the particles. As shown in Fig. 13, $\pi^{\pm}/K^{\pm}/p^{\pm}/\bar{d}$ particles are distinctly separated from each other, enabling precise identification of reacted particles.

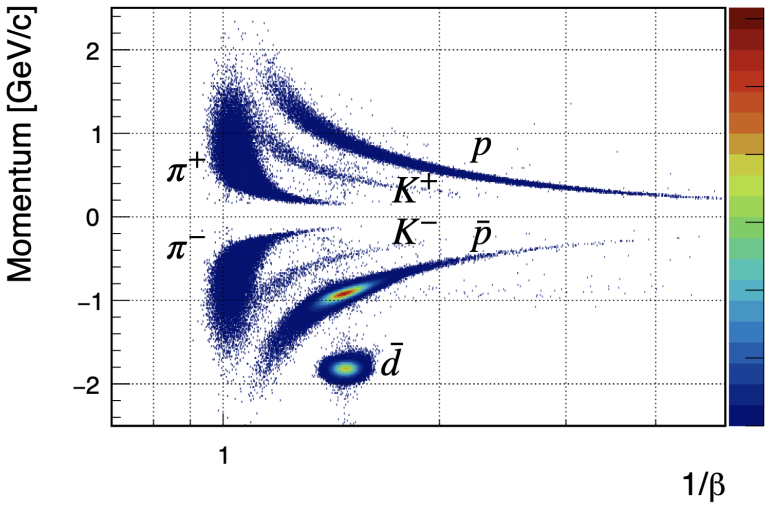

Figure 13: Particle identification for reconstructed events. $\pi^{\pm}/K^{\pm}/p^{\pm}/\bar{d}$ can be clearly separated.

4.1 Derive $\bar{d}$−nucleus Optical Potential

Track multiplicity and decomposition are depicted in Fig. 14. A distance of the closest approach (DCA) based vertex cut has been applied to the track reconstruction to suppress combinatorial background due to large multiplicity. Only the combination that gives the smallest summed DCA is considered as the current reconstructed vertex.

The multiplicity distribution with one $\bar{p}$ detected by the forward TOF wall is used to calibrate the charge multiplicity for part of the partial annihilation events. The complete multiplicity distribution for partial annihilation can be obtained by adding back the events where $\bar{n}$ flies out, which can be achieved by shifting the $\bar{p}$ event multiplicity by -1. The multiplicity distribution for coherent annihilation can then be derived by adding a gaussian fit function to fit the total multiplicity distribution as given in magenta line in Fig. 14, where the cyan shows the over all fit function. The yield for both partial and coherent annihilation can be obtained by integrating the fitted functions. Our simulation demonstrates a precision better than 20% for the multiplicity decomposition and thus $\sigma_{ParAnn}/\sigma_{CohAnn}$ precision.

Another uncertainty for σ_{ParAnn} and σ_{CohAnn} measurement arises from misidentification of successive partial annihilation events within the vertex resolution as coherent annihilation. To suppress this effect, we propose using a sliced thin graphite target with 1 cm thickness, as successive partial annihilation within the same target slice can be suppressed to less than 5%. Considering other sources of ambiguity such as bias and efficiency in identifying annihilation events, we anticipate achieving an overall experimental precision of approximately 20% based on our simulations. When we apply this

result to derive the strength of the $\bar{d}$–^{12}C interaction by comparing with GiBUU calculation, we can expect a precision of $\sim 20\%$ for the real part of the optical potential as final results.

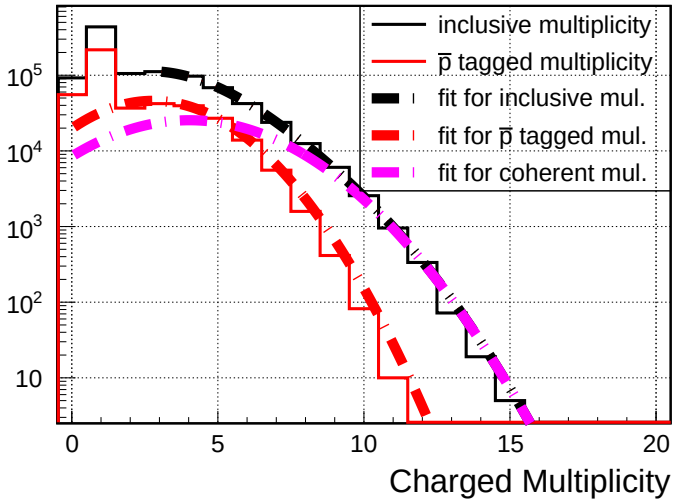

Figure 14: Inclusive charge multiplicity (black) is decomposed into partial and coherent contributions, which are fitted to derive σ_{ParAnn} (red) and σ_{CohAnn} (magenta) annihilation cross sections.

4.2 Distinguish Multiple $\bar{N} - N$ Annihilation Mechanism

As previously discussed, the π momentum distribution can be used to distinguish between the three annihilation scenarios because the kinematic constraints governing the π momentum distribution are directly linked to the annihilation phase space. After selecting reconstructed $\pi^{\pm}$ based on PID as shown in Fig. 13, we find that the final acceptance for charged π with momentum ≥ 1.6 GeV/c is approximately 30%.

After event selection, the final charged $\pi^{\pm}$ momentum distribution including experimental resolution and energy loss inside graphite target for partial and coherent annihilation events is shown in Fig. 15 and 16, respectively. The π momentum distribution for partial annihilation events shows a slight excess of π momentum than 1.6 GeV/c due to the Fermi motion contribution. The π momentum distribution for coherent annihilation events shows 5 times more events above the kinematic limit as a result of the Correlated Cascade Annihilation from GiBUU. Please note that the One-Step Simultaneous Annihilation is not included in the current GiBUU calculation, which will contribute $2 \sim 3$ times more events above the kinematic limit than the Correlated Cascade Annihilation by assuming a 20% of SRC states for both $\bar{d}$ and ^{12}C nucleus.

As a result, we expect to detect ~ 500 $\pi^{\pm}$ with momentum ≥ 1.6 GeV/c from both Cascade Correlated Annihilation and One-Step Simultaneous Annihilation combined, which is one order of magnitude more than the Fermi motion contribution. This statistics will allow us to identify the existence of the Correlated Cascade Annihilation and One-Step Simultaneous Annihilation events with 20σ significance. Further decoupling between the these two scenarios can be achieved by fitting the $\pi^{\pm}$ momentum distribution with phase space distribution as described in Section 2.2.

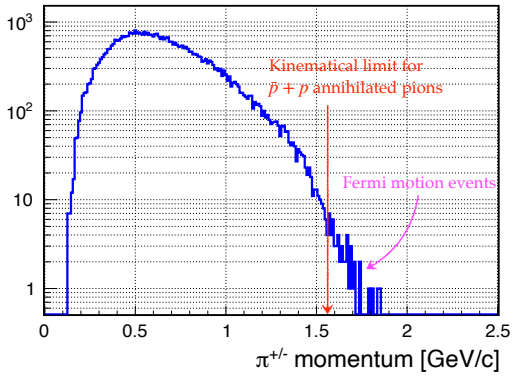

Figure 15: π momentum distribution from $\bar{d}$+^{12}C partial annihilation events after event selection.

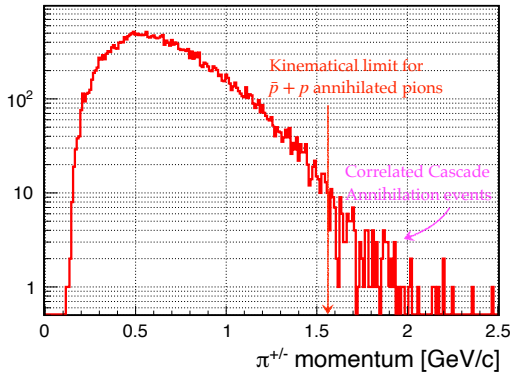

Figure 16: π momentum distribution from $\bar{d}$+^{12}C coherent annihilation events after event selection.

5 Summary

We propose to investigate the antideuteron physics at J-PARC K1.8 beam line as a first step towards study antimatter composed of multiple antinucleons. The main topics to be addressed are the $\bar{d}$−nucleus optical potential and the multiple $\bar{N}-N$ annihilation mechanism. The effectiveness of the proposed method is demonstrated through calculations using the GiBUU package. An optimized experimental setup is proposed. The acceptance and resolution of the experimental setup are estimated using GEANT4 simulations, and the performance of the proposed method is evaluated.

The proposed experiment will determine the $\bar{d}$–^{12}C optical potential and identify contributions from different annihilation mechanisms. These measurements will provide the first direct constraints on QCD matter in the low-temperature, high-density region of the phase diagram—complementary to heavy-ion collisions and neutron-star observations—while establishing a foundation for future studies of heavier antinuclei.

References

[1] E. Widmann *et al.*, Hyperfine Interact. 240 (2019) 5

[2] The STAR Collaboration, Nature Physics 16 (2020) 409

[3] Angles & Demons (2009) directed by R. Howard, Columbia Pictures

[4] Th. Walcher *et al.*, Ann. Rev. Nucl. Part. Sci. 38 (1988) 67

[5] F. Binon *et al.*, Phys. Lett. B 31 (1970) 230

[6] S. P. Denisov *et al.*, Nucl. Phys. B 31 (1971) 253

[7] S. Acharya *et al.*, Phys. Rev. Lett. 125 (2020) 162001

[8] O. Chamberlain *et al.*, Phys. Rev. 100 (1955) 947

[9] A. B. Larionov *et al.*, Phys. Rev. C 80 (2009) 021601

[10] E. Friedman *et al.*, Nucl. Phys. A 761 (2005) 283

[11] C. J. Batty, Rep. Prog. Phys. 52 (1989) 1165

[12] D. Garreta, *et al.*, Phys. Lett. 149B (1984) 64

[13] R. Subedi, *et al.*, Science 320 (2008) 1476

[14] M. Ukai, *et al.*, arXiv:2312.11821

[15] F. Iazzi, Nucl. Phys. A 655 (1999) 371c

[16] J. R. Sanford and C. L Wang, BNL report 11479 (1967)

[17] C. Van Der Leun and C. Alderliesten, Nucl. Phys. A 380 (1982) 261

[18] E. H. Auerbach, *et al.*, Phys. Rev. Lett. 46 (1981) 702

[19] V. Flaminio *et al.*, CERN-HERA 84-01 (1984)

[20] I. Tanihata, *et al.*, Phys. Rev. Lett. 55 (1985) 2676

[21] R. B. Wiringa, V. G. J. Stoks, and R. Schiavilla, Phys. Rev. C 51 (1995) 38

[22] A. B. Larionov *et al.*, Phys. Rev. C 78 (2008) 014604

[23] O. Buss *et al.*, Phys. Rep. 512, (2012) 1

[24] S. Hayakawa, PhD thesis, Osaka University, (2019)